Membrane potential is vital for rapid permeabilization of plasma membranes and lipid bilayers by the antimicrobial peptide lactoferricin B

Received for publication, January 28, 2019, and in revised form, May 17, 2019 Published, Papers in Press, May 22, 2019, DOI 10.1074/jbc.RA119.007762

Farzana Hossain[‡], **Md. Mizanur Rahman Moghal**[‡], **Md. Zahidul Islam**[‡1], **Md. Moniruzzaman**[‡], **and Masahito Yamazaki**[‡§¶2]

From the [‡]*Integrated Bioscience Section, Graduate School of Science and Technology, Shizuoka University, Shizuoka 422-8529, the* [§]*Nanomaterials Research Division, Research Institute of Electronics, Shizuoka University, Shizuoka 422-8529, and the* [¶]*Department of Physics, Graduate School of Science, Shizuoka University, Shizuoka 422-8529, Japan*

Edited by Karen G. Fleming

Lactoferricin B (LfcinB) is a cationic antimicrobial peptide, and its capacity to damage the bacterial plasma membrane is suggested to be a main factor in LfcinB's antimicrobial activity. However, the specific processes and mechanisms in LfcinB-induced membrane damage are unclear. In this report, using confocal laser-scanning microscopy, we examined the interaction of LfcinB with single *Escherichia coli* cells and spheroplasts containing the water-soluble fluorescent probe calcein in the cytoplasm. LfcinB induced rapid calcein leakage from single *E. coli* cells and from single spheroplasts, indicating that LfcinB interacts directly with the plasma membrane and induces its rapid permeabilization. The proton ionophore carbonyl cyanide *m*-chlorophenylhydrazone suppressed this leakage. Next, we used the single giant unilamellar vesicle (GUV) method to examine LfcinB's interaction with GUVs comprising polar lipid extracts of *E. coli* containing a water-soluble fluorescent probe, Alexa Fluor 647 hydrazide (AF647). We observed that LfcinB stochastically induces local rupture in single GUVs, causing rapid AF647 leakage; however, higher LfcinB concentrations were required for AF647 leakage from GUVs than from *E. coli* cells and spheroplasts. To identify the reason for this difference, we examined the effect of membrane potential on LfcinB-induced pore formation, finding that the rate of LfcinB-induced local rupture in GUVs increases greatly with increasing negative membrane potential. These results indicate that membrane potential plays an important role in LfcinB-induced local rupture of lipid bilayers and rapid permeabilization of *E. coli* plasma membranes. On the basis of these results, we discuss the mode of action of LfcinB's antimicrobial activity.

Lactoferricin B (LfcinB)[3] is produced by the hydrolysis of transferrin-like bovine lactoferrin in milk (*e.g.* pepsin digestion in the human stomach) (1, 2), which has antimicrobial activities against Gram-negative and -positive bacteria, yeast, and filamentous fungi (2–4), and hence, LfcinB is one of the antimicrobial peptides (AMPs). LfcinB is a 25-residue cationic peptide (FKCRRWQWRMKKLGAPSITCVRRAF) with 5 Arg residues and three Lys residues (3). The three-dimensional LfcinB structure exhibits an amphipathic character because one surface of the peptide is hydrophobic, whereas its opposite surface is hydrophilic (5). This amphipathic character of the three-dimensional structure of peptides is common to most AMPs (6–10). Shorter versions of LfcinB also have antimicrobial activity (4, 11–15). A shorter version of LfcinB composed entirely of D amino acid residues had the same antibacterial activity as that composed of natural L amino acid residues (16, 17), indicating that proteins are not involved in the antibacterial activity of this peptide.

In our previous paper (18), we investigated the interaction of LfcinB with single giant unilamellar vesicles (GUVs) composed of negatively-charged dioleoylphosphatidylglycerol (DOPG) and electrically neutral dioleoylphosphatidylcholine (DOPC) mixtures containing a water-soluble fluorescent probe, calcein, in their lumen using the single GUV method (18). It is well-known that using the single GUV method we can separate a process of AMP-induced damage of a membrane such as pore formation from a process of leakage (membrane permeation) of fluorescent probes through the damage (19). At the beginning of the interaction of LfcinB with a single GUV, the calcein concentration in the GUV lumen remained constant, but suddenly calcein started to leak from the GUV and the leakage completed within 5 s after starting the leakage, with a concomitant

This work was supported in part by Grant-in-Aid for Scientific Research (B) numbers 15H04361 and 19H03193 from the Japan Society for the Promotion of Science (JSPS) (to M. Y.) and the Cooperative Research Project of Research Center for Biomedical Engineering. The authors declare that they have no conflicts of interest with the contents of this article.

This article contains Figs. S1–S2.

[1] Present address: Dept. of Biotechnology and Genetic Engineering, Jahangirnagar University, Savar, Dhaka-1342, Bangladesh.

[2] To whom correspondence should be addressed: Nanomaterials Research Division, Research Institute of Electronics, Shizuoka University, 836 Oya, Suruga-ku, Shizuoka 422-8529, Japan. Tel./Fax: 81-54-238-4741; E-mail: yamazaki.masahito@shizuoka.ac.jp.

[3] The abbreviations used are: LfcinB, lactoferricin B; GUV, giant unilamellar vesicle; AF647, Alexa Fluor 647 hydrazide; AMPs, antimicrobial peptides; DOPG, dioleoylphosphatidylglycerol; DOPC, dioleoylphosphatidylcholine; CLSM, confocal laser scanning microscopy; FI, fluorescence intensity; MIC, minimum inhibitory concentration; calcein-AM, calcein-acetoxymethyl; CCCP, carbonyl cyanide *m*-chlorophenylhydrazone; $\Delta\varphi$, membrane potential; $P_{leak}(t)$, the fraction of leaked cells among all examined cells over time t; DIC, differential interference contrast; $P_{intact}(t)$, fraction of intact GUVs among the examined GUVs over time t; k_P, rate constant of the LfcinB-induced local rupture; TEAC, tetraethylammonium chloride; $DiOC_6(3)$, 3,3′-dihexyloxacarbocyanine iodide.

decrease in GUV size. We performed the same experiments using many "single GUVs," and found that the leakage started at different times in all GUVs but the time required for complete leakage after starting was less than 5 s in all GUVs. To express the LfcinB-induced membrane damage inducing this rapid leakage, we used the term "local rupture" instead of "large pore." Moreover, in the interaction of LfcinB with *Escherichia coli* cell suspension in the presence of a membrane-impermeant fluorescent probe, SYTOX Green, it was observed that the fluorescence intensity of SYTOX Green of the suspension increased gradually with time, suggesting LfcinB-induced influx of SYTOX Green from the outside of *E. coli* into the cytoplasm (18). These results suggest that LfcinB-induced plasma membrane damage is a main factor in its antimicrobial activity. However, experimental data demonstrating the direct interaction of LfcinB with single bacterial cells is needed.

In the present study, we examined the interaction of LfcinB with single *E. coli* cells to reveal the mechanism of its antimicrobial activity. For this purpose, we investigated the interaction of LfcinB with live single *E. coli* cells containing calcein in the cytoplasm using confocal laser scanning microscopy (CLSM). We found that LfcinB induced rapid leakage of calcein from single *E. coli* cells, indicating that LfcinB induced rapid permeabilization due to damage or pore formation in the plasma membrane. Gram-negative bacteria such as *E. coli* are composed of an outer membrane, a peptidoglycan layer, and a plasma membrane (inner membrane); hence, there may be several targets of LfcinB. To examine whether direct interaction of LfcinB with the plasma membrane plays a role in the calcein leakage, we investigated the interaction of LfcinB with single spheroplasts derived from *E. coli* cells using CLSM. Spheroplasts do not have an outer membrane and peptidoglycan, and hence only the plasma membrane and cytoplasm remain (20–23). We prepared spheroplasts from filamentous *E. coli* cells and loaded calcein in the cytoplasm. We found that LfcinB induced rapid leakage of calcein from single spheroplasts. To elucidate the elementary processes and the mechanism of LfcinB-induced damage of the plasma membrane, we examined the interactions of LfcinB with GUVs of *E. coli* polar lipid extract (*E. coli*-lipid) using the single GUV method (19, 24–26). LfcinB induced stochastic local rupture in *E. coli*-lipid-GUVs, but higher concentrations of LfcinB were required to induce a significant rate of local rupture compared with that observed in *E. coli* cells and spheroplasts. We hypothesized that this difference is due to the membrane potential in the cells and spheroplasts, because the membrane potential of *E. coli* cells is $-100 \sim -130$ mV at pH 6.0∼7.0 (27) and it is expected that the negative membrane potential could affect the interaction of highly positively charged LfcinB with the plasma membrane due to strong electrostatic interactions. To verify this hypothesis, we examined the effect of membrane potential on LfcinB-induced local rupture or pore formation in single GUVs and also the effect of a proton ionophore, carbonyl cyanide *m*-chlorophenylhydrazone on the LfcinB-induced leakage of calcein from single *E. coli* cells and spheroplasts. On the basis of these results, we discuss the mode of action of LfcinB's antimicrobial activity.

Results

Interaction of LfcinB with single E. coli cells

To elucidate the mechanism of action of LfcinB in live bacterial cells, we examined the interaction of LfcinB with single live *E. coli* cells in EZ rich medium using CLSM. EZ medium is a synthetic cell culture medium, allowing us to control for unexpected interactions of peptides with unknown components contained in most media (28). We loaded calcein to the cytoplasm of *E. coli* cells, using the interaction between calcein-AM and *E. coli* cells. It is well-known that hydrophobic calcein-AM can pass through the plasma membrane to enter the cytoplasm of bacterial cells, where it is hydrolyzed by esterases to produce calcein (29, 30). We applied the same method to load calcein in *E. coli* spheroplasts, and successfully loaded spheroplasts with calcein (see the next section), indicating the validity of the above interpretation.

First, we investigated the interaction of 3.0 μM LfcinB with single *E. coli* cells in EZ rich medium in a microchamber at 25 °C. Under this condition before the interaction of LfcinB, *E. coli* cells grew and the average increase in cell length for 10 min was 11 ± 3%. A LfcinB solution was continuously provided to the vicinity of an *E. coli* cell through a micropipette, so that the LfcinB concentration near the cell became constant at a steady state, and was almost the same as that in the micropipette (31). Two kinds of cells were present, nonseptating and septating cells. Fig. 1*A* shows a typical result for septating cells. During the interaction of 3.0 μM LfcinB, the fluorescence intensity (FI) of the cell due to calcein was constant during the initial interaction (up to 26 s), then rapidly decreased (Fig. 1*A*, and *green line* in *C* and *D*), indicating that LfcinB induced rapid permeabilization. This is due to LfcinB-induced damage or pore formation in the plasma membrane through which calcein leaked rapidly. On the other hand, the length of the cell increased before the addition of LfcinB (6% increase for 10 min), but subsequently the length gradually decreased (7% decrease for 6 min after the start of the interaction) (*red squares* in Fig. 1, *C* and *D*). The same experiments were performed using 10 cells (*i.e.* 7 nonseptating and 3 septating cells), and the same result (*i.e.* first a rapid leakage of calcein occurred, then a gradual decrease in cell length) was observed in 7 cells (*i.e.* 5 nonseptating and 2 septating cells). Thus, the fraction of LfcinB-induced leaked cells among all examined cells after 6 min reaction (P_{leak} (6 min)), which is a measure of the rate of pore formation or local rupture induced by peptides (24, 32), was 0.70 for 3.0 μM LfcinB. We conducted five independent experiments ($n = 5$) for the 3.0 μM LfcinB concentration, and obtained the mean ± S.D. of the fraction of leaked cell. P_{leak} for 3.0 μM LfcinB was 0.71 ± 0.05. Fig. 1*E* shows the time course of FI of several cells during the interaction of 3.0 μM LfcinB. Each curve corresponds to the time course of FI for each cell. This result indicates a wide distribution of rates of LfcinB-induced leakage of calcein from a single cell. The rate of leakage in septating cells was larger than that in nonseptating cells. To compare the rate more quantitatively, we estimated the rate of LfcinB-induced leakage of calcein from a single cell using half-time (*i.e.* $t_{1/2}$), which is defined as the time required for leakage of 50% of total calcein from a single cell after the start of the leak-

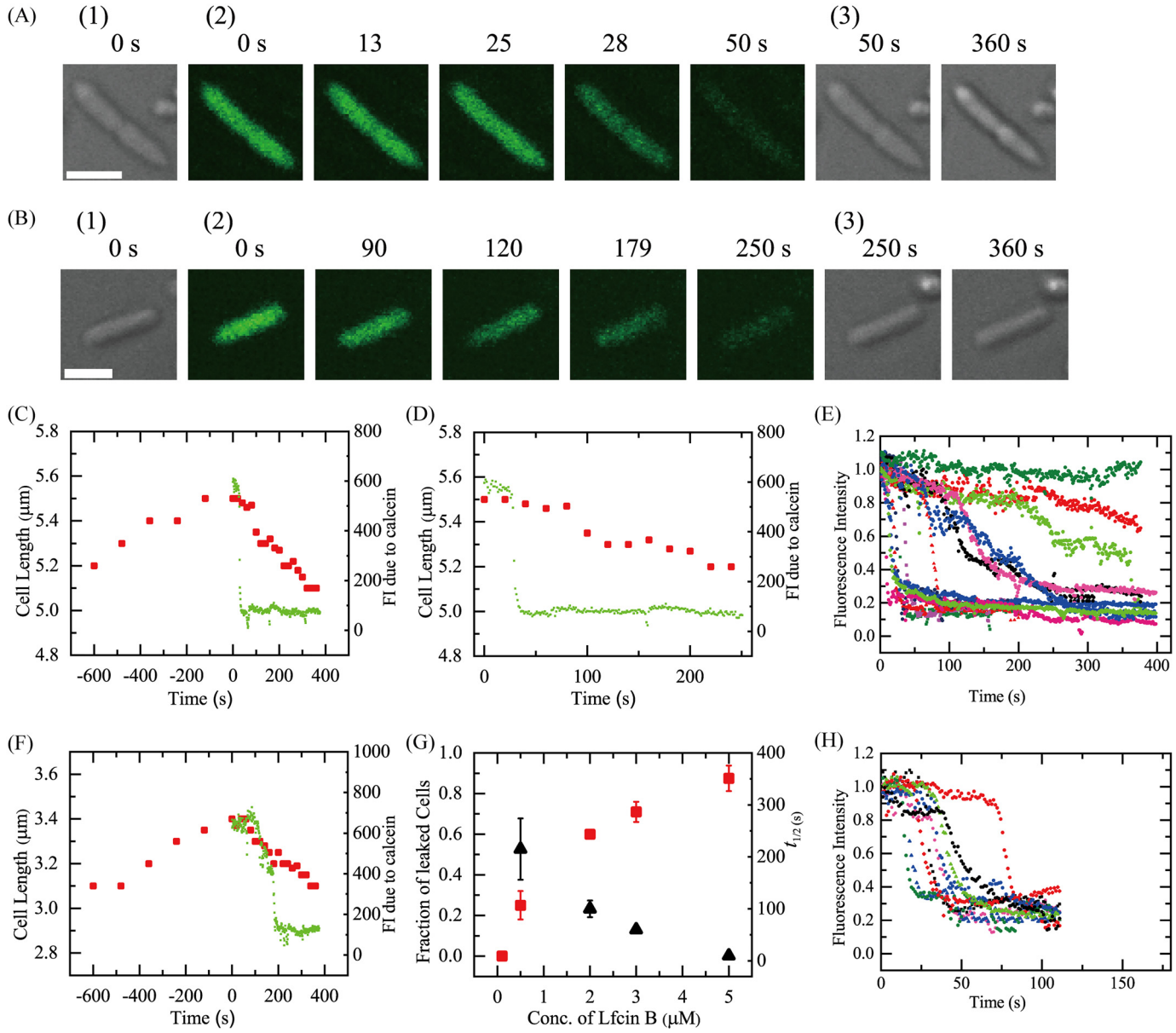

Figure 1. Interactions of LfcinB with single *E. coli* cells containing calcein. *A* and *B*, CLSM images due to calcein (images with *green color*) (*2*) and DIC images (*1* and *3*). The *number above* each image shows the time in seconds after the addition of (*A*) 3.0 μM and (*B*) 0.5 μM LfcinB was started. The *bar* is 2.0 μm. *C* and *D*, the time course of change in the FI of the total cell due to calcein and cell length during the interaction of 3.0 μM LfcinB at 25 °C in *A*. The addition of LfcinB was started at $t = 0$. *Green lines* correspond to the FI of calcein, and *red squares* represent cell length. *D*, an expanded figure of *C* after $t = 0$. *E*, other examples of the time course of the change in the normalized FI of several "single cells" under the same conditions as in *A*. *F*, the time course of change in the FI of the total cell due to calcein and its length during the interaction of 0.5 μM LfcinB in *B*. The addition of LfcinB was started at $t = 0$. *Green lines* correspond to the FI of calcein, and *red squares* represent cell length. *G*, LfcinB concentration dependence of the fraction of leaked cells after 6 min interaction (*red* ■) and the leakage half-time (▲). Mean ± S.D. of the fraction of leaked cells (or S.E. values of leakage half-time) are shown. *H*, time course of the change in the normalized FI of several single cells during the interaction of 5.0 μM LfcinB.

age. We plotted the distribution of $t_{1/2}$ using a histogram (Fig. S1). This indicates that the $t_{1/2}$ values of all septating cells ($n = 28$) were less than 50 s, but the $t_{1/2}$ values of nonseptating cells ($n = 44$) was widely distributed from 6 to 259 s. This quantitative analysis supports the conclusion that the rates of leakage from septating cells were larger than those from most nonseptating cells and there is a wide distribution of the rates of leakage from nonseptating cells.

Before the interaction of LfcinB the cell length of *E. coli* cells increased, but after the start of the interaction of LfcinB the cell length started to decrease, indicating that the LfcinB-induced leakage from cells stopped cell growth. These results indicate that first LfcinB induced permeabilization in plasma membrane of *E. coli* cells due to damage or pore formation in the plasma membrane, through which calcein rapidly leaked, and then cell growth stopped, resulting in a decrease in cell length. A similar decrease in the cell length of *E. coli* cells was reported for the AMP, LL-37 (33).

Next, we investigated the interaction of a lower concentration (0.5 μM) of LfcinB with single *E. coli* cells in the medium at 25 °C. Fig. 1*B* shows a typical result for nonseptating cells. During the interaction of 0.5 μM LfcinB, the FI of a cell due to

calcein was constant initially (up to 110 s), and then gradually decreased (Fig. 1*B*, and *green line* in *F*), indicating that LfcinB induced rapid permeabilization due to damage or pore formation in the plasma membrane through which calcein leaked. On the other hand, cell length increased before the interaction of LfcinB (10% increase for 10 min), but subsequently cell length gradually decreased (9% decrease for 6 min) (*red squares* in Fig. 1*F*).

Fig. 1*G* shows the LfcinB concentration dependence of P_{leak} (6 min). At 0.1 μM, no leakage was observed (*i.e.* $P_{leak} = 0$), whereas at and above 0.5 μM, the P_{leak} increased with an increase in LfcinB concentration. This result indicates that the rate of damage or pore formation in the plasma membrane of *E. coli* cells increased in a LfcinB concentration-dependent manner. On the other hand, the rate of LfcinB-induced leakage of calcein through damages or pores also greatly depended on LfcinB concentration. Fig. 1*H* shows the time course of FI of several cells due to calcein among all examined cells ($n = 17$ for 2 independent experiments) during the interaction of 5.0 μM LfcinB, indicating that LfcinB induced leakage of calcein from a single cell at a great rate and the values of this rate exhibited a sharp distribution. The mean ± S.E. of leakage half-time ($t_{1/2}$) were obtained for each LfcinB concentration (the number of cells, n, was 15–17, except for 3.0 μM ($n = 72$) and 0.5 μM ($n = 5$)) (Fig. 1*G*). For example, $t_{1/2}$ for 2 and 5 μM LfcinB was 100 ± 20 and 10 ± 1 s, respectively. Leakage half-time decreased with an increase in LfcinB concentration (Fig. 1*G*), indicating that the rate of leakage from the pores increased in an LfcinB concentration-dependent manner.

It is reported that the minimum inhibitory concentration (MIC) of LfcinB against *E. coli* (JM-109) is 3 ± 1 μM (18). For measurement of MIC, we use a suspension of many *E. coli* cells. As the interaction of LfcinB with many cells proceeds, the effective LfcinB concentration outside the cells decreases. For example, if we use 3 μM LfcinB initially, the effective concentration outside the cells is smaller than 3 μM. Moreover, the MIC values are determined after ~20 h culture. In contrast, in the experiments of interaction of LfcinB with the single *E. coli* cells described above, we continuously add LfcinB solution, and hence the LfcinB concentration remains constant from the beginning (*e.g.* 3 μM). Therefore, LfcinB concentration near *E. coli* cells in a single cell experiment is larger than that in the MIC measurement using a suspension of cells. This is the reason why P_{leak} (6 min) was large for 3.0 μM LfcinB. To compare quantitatively the result of single cell experiments shown in Fig. 1 and that of MIC measurement, we need a systematic investigation in the near future.

To elucidate the role of membrane potential in the interaction of LfcinB with single live *E. coli* cells, we investigated the effect of a proton ionophore, CCCP, on the interaction of LfcinB with the cells. It is well-known that CCCP decreases the transmembrane difference of the electrochemical potential of proton (or the proton-motive force) in the plasma membrane of bacterial cells, such as *E. coli*, by increasing proton permeability in the membrane, dissipating the membrane potential, $\Delta\varphi$, as well as the transmembrane pH difference, ΔpH (34). If the pH of the external medium is neutral, ΔpH is small (27). The pH of EZ medium used in the above experiments is pH 7.0, and hence,

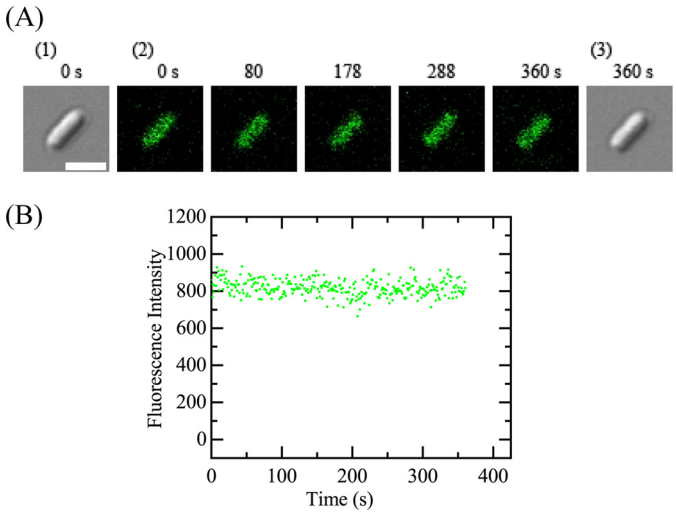

Figure 2. Interactions of LfcinB with single *E. coli* cells containing calcein in the presence of CCCP. *A,* CLSM images due to calcein (images with *green color*) (*2*) and DIC images (*1* and *3*). The *number above* each image shows the time in seconds after the addition of 5.0 μM was started. The *bar* is 2.0 μm. *B,* the time course of change in the FI of the total cell due to calcein during the interaction of 5.0 μM LfcinB at 25 °C in *A*. The addition of LfcinB was started at $t = 0$.

we can consider that CCCP mainly dissipated $\Delta\varphi$ under our experimental conditions.

In the presence of 100 μM CCCP in the EZ medium (final concentration), we investigated the interaction of 5.0 μM LfcinB with single *E. coli* cells in the medium at 25 °C. The FI of the cell due to calcein was constant during the interaction (up to 6 min) (Fig. 2, *A* and *B*), indicating LfcinB did not induce any damage in the plasma membrane through which calcein leaked. The same experiments were performed using 12 cells (*i.e.* 10 nonseptating and 2 septating cells), and the same result was observed. We conducted two independent experiments using 12–15 *E. coli* cells ($n = 2$), and obtained the same results. These results indicate that membrane potential in the plasma membrane plays an important role in LfcinB-induced permeabilization due to damage or pore formation in the plasma membrane of *E. coli* cells.

Interaction of LfcinB with single E. coli spheroplasts

To examine the direct interaction of LfcinB with the plasma membrane of *E. coli* cells, we investigated the interaction of LfcinB with single spheroplasts derived from *E. coli* cells using CLSM. We loaded calcein in the lumen of spheroplasts by interacting calcein-AM with spheroplasts using the same method used for *E. coli* cells, as described in the previous section.

First, we investigated the interaction of 2.0 μM LfcinB with single spheroplasts in 10 mM Tris-HCl (pH 7.8) containing 1.5 mM KCl, 48.5 mM NaCl, and 0.73 M sucrose at 25 °C (the concentrations of K^+ and Na^+ are almost the same as those in the EZ rich medium). A LfcinB solution was continuously provided to the vicinity of a spheroplast through a micropipette. During the interaction of 2.0 μM LfcinB, the FI of the spheroplast lumen due to calcein was constant up to 66 s, and then rapidly decreased to zero within a few seconds (Fig. 3, *A* and *B*), indicating that LfcinB induced rapid permeabilization due to damage or pore formation in the plasma membrane of the sphero-

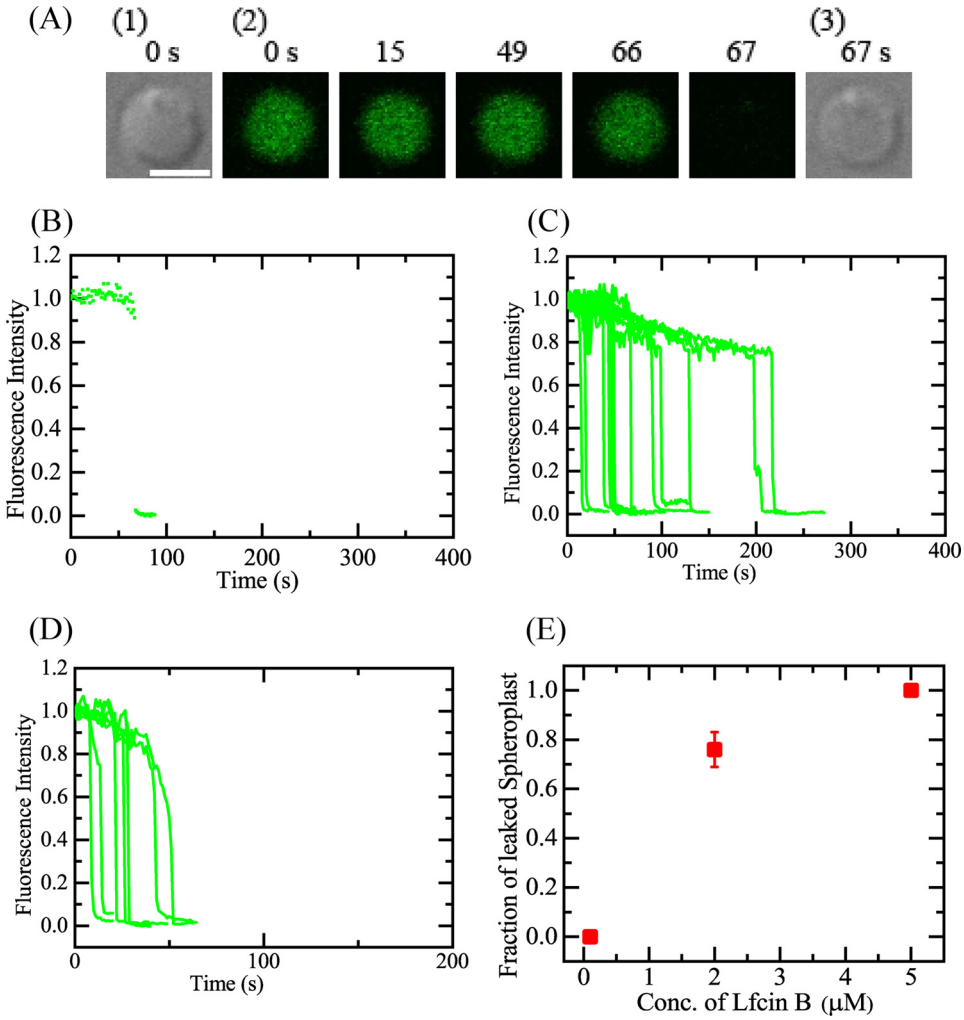

Figure 3. Interactions of LfcinB with single spheroplasts containing calcein. *A,* CLSM images due to calcein (images with *green color*) (*2*) and DIC images (*1* and *3*). The *number above* each image shows the time in seconds after the addition of 2.0 μM LfcinB was started. The *bar* is 5.0 μm. *B,* the time course of change in the normalized FI of the total spheroplast due to calcein during the interaction of 2.0 μM LfcinB at 25 °C shown in *A*. We obtained the normalized FI of a spheroplast as the ratio of the FI at time *t* to that before the addition of LfcinB. The addition of LfcinB was started at $t = 0$. *C,* other examples of the time course of the change in the normalized FI of several spheroplasts under the same experimental conditions as in *A*. *D,* the time course of change in the normalized FI of the spheroplasts due to calcein during the interaction of 5.0 μM LfcinB. In *C* and *D*, each curve corresponds to the time course of FI of each spheroplast. *E,* LfcinB concentration dependence of the fraction of leaked spheroplasts (*red* ■). Mean ± S.D. of the fraction of leaked spheroplasts are shown.

plast through which calcein leaked. When we performed the same experiments using other spheroplasts, similar rapid leakage of calcein occurred stochastically within 6 min after a gradual decrease in FI (Fig. 3*C*). This initial gradual decrease in FI was also observed in spheroplasts in the absence of LfcinB, and hence we can consider reasonably that it is due to the photobleaching of calcein (Fig. 3*C*). For 2.0 μM LfcinB, 13 spheroplasts exhibited leakage by 6 min among all examined ones ($n = 16$) (*i.e.* P_{leak} (6 min) = 0.81).

Next, we investigated the interaction of higher concentrations of LfcinB with single spheroplasts at 25 °C. During the interaction of 5.0 μM LfcinB, the FI of spheroplasts due to calcein was constant, and then rapidly decreased (Fig. 3*D*), indicating that LfcinB induced rapid permeabilization due to damage or pore formation in the plasma membrane of the spheroplasts. Fig. 3*E* shows the LfcinB concentration dependence of P_{leak} (6 min). We conducted two independent experiments for each LfcinB concentration, and obtained the mean ± S.D. of the fraction of leaked spheroplast. At 0.1 μM, no leakage was observed (*i.e.* $P_{leak} = 0$), whereas at 2.0 μM, $P_{leak} = 0.76 \pm 0.07$, and at 5.0 μM, $P_{leak} = 1.0$; thus, P_{leak} increased in an LfcinB concentration-dependent manner. This result indicates that the rate of damage or pore formation in the plasma membrane of spheroplasts increased with an increase in LfcinB concentration.

These results indicate that the direct interaction of LfcinB with the plasma membrane of spheroplasts induces rapid permeabilization due to damage or pore formation in the membrane, through which the internal contents rapidly leak. The dependence of the fraction of leaked spheroplast for 6 min on the LfcinB concentration was similar to that of *E. coli* cells, indicating that one of the targets of LfcinB in *E. coli* cells is the plasma membrane. In contrast, the time course of the LfcinB-induced leakage from spheroplasts was different from that of *E. coli* cells. The starting time and the rate of leakage in *E. coli* cells was slower and had a wider distribution compared with that in spheroplasts. This difference can be explained as follows. In *E. coli* cells, LfcinB molecules must pass through the outer membrane and peptidoglycan layer in the periplasm to

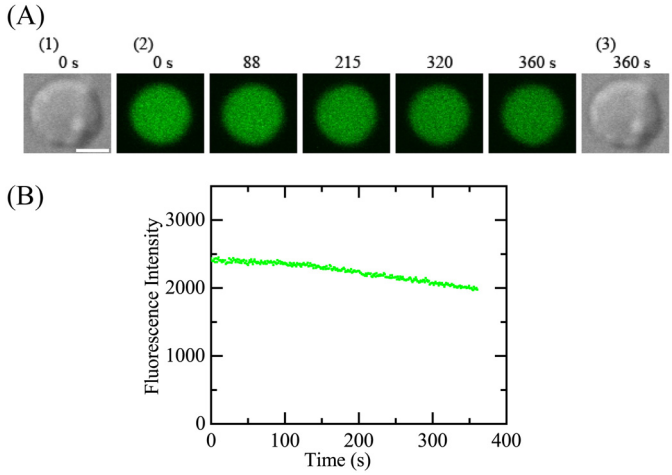

Figure 4. Interactions of LfcinB with a single spheroplast containing calcein in the presence of CCCP. *A,* CLSM images due to calcein (images with *green color*) (*2*) and DIC images (*1* and *3*). The *number above* each image shows the time in seconds after the addition of 5.0 μM was started. The *bar* is 5.0 μm. *B,* the time course of change in the FI of the total cell due to calcein during the interaction of 5.0 μM LfcinB at 25 °C in *A*. The addition of LfcinB was started at $t = 0$.

reach the plasma membrane, which decreases and varies the rate of increase in LfcinB concentration in the plasma membrane. Moreover, for the leakage of calcein molecules to the outside of the cells, they must pass through the peptidoglycan layer and the outer membrane, which decreases and varies the rate of leakage of calcein. Therefore, the difference of the time course of the leakage is due to the barriers (*i.e.* the peptidoglycan layer and the outer membrane) of the cells.

Several experimental results indicate that spheroplasts from *E. coli* cells have membrane potential (35). To elucidate the role of membrane potential in the interaction of LfcinB with single spheroplasts, we examined the effect of a CCCP on the interaction of LfcinB with the spheroplasts. In the presence of 100 μM CCCP in 10 mM Tris-HCl (pH 7.8) containing 1.5 mM KCl, 48.5 mM NaCl, and 0.73 M sucrose, we investigated the interaction of 5.0 μM LfcinB with single spheroplasts at 25 °C. A gradual decrease in FI occurred during the interaction (up to 6 min) (Fig. 4, *A* and *B*) due to the photobleaching of calcein, indicating LfcinB did not induce any damage in the plasma membrane through which calcein leaked. The same experiments were performed using 15 spheroplasts, and the same result was observed (*i.e.* $P_{leak} = 0$). We conducted two independent experiments using 15 spheroplasts ($n = 2$), and obtained the same results. This result indicates that the membrane potential in the spheroplasts plays an important role in the LfcinB-induced rapid permeabilization due to damage or pore formation in their membranes.

Interaction of LfcinB with single E. coli-lipid-GUVs

To elucidate the interaction of LfcinB with the *E. coli* plasma membrane, we prepared GUVs of lipid bilayers with a lipid composition similar to the *E. coli* plasma membrane and examined the interaction of LfcinB with these GUVs using the single GUV method. For this purpose, we used an *E. coli* polar lipid extract (*E. coli*-lipid), whose lipid composition is phosphatidylethanolamine/phosphatidylglycerol/cardiolipin (67/23/10 (weight % ratio)). We first investigated the interaction of LfcinB with single *E. coli*-lipid-GUVs containing a water-soluble fluorescent probe, AF647. For the GUV experiments, buffer C (10 mM PIPES, pH 7.0, 1 mM EGTA, 50 mM NaCl) was used. Fig. 5*A* shows a typical experimental result of the interaction of 40 μM LfcinB with single GUVs. The FI of the GUV lumen due to AF647 remained essentially constant during the addition of LfcinB solution for the first 124 s, then the FI rapidly decreased (Fig. 5, *A*(*2*) and *B*). At 125 s, the FI fell to effectively zero; a differential interference contrast (DIC) image of the same GUV (Fig. 5*A*(*3*)) showed that the spherical GUV structure remained, albeit with an apparent decrease in diameter. This is essentially the same phenomenon as that observed in the interaction of LfcinB with DOPG/DOPC (1/1)-GUVs (18). As discussed in our previous report (18), the rapid decrease in FI occurred as a result of the rapid leakage of the fluorescent probe through the LfcinB-induced local rupture of the GUV. Thus, the time at which the FI began to rapidly decrease corresponded red to the time at which local rupture occurred in the GUV. When the same experiments were carried out using 12 single GUVs, we observed the stochastic occurrence of a similar rapid leakage of AF647 from each GUV (Fig. 5*C*).

As demonstrated in our previous studies on peptide-induced damages in GUV membranes (18, 25), the rate constant of LfcinB-induced pore formation or local rupture in the membrane can be obtained by analyzing the time course of the fraction of intact GUVs (*i.e.* those from which the fluorescent probe did not leak) among the examined GUVs, $P_{intact}(t)$, over time t. Fig. 5*D* shows that the value of P_{intact} of *E. coli*-lipid-GUVs decreased with time during the interaction of 40 μM LfcinB. If we assume a two-state transition from the intact state to the locally ruptured state of single GUVs, we can obtain the theoretical equation of the time course of $P_{intact}(t)$ as follows (18, 25),

$$P_{intact}(t) = \exp\{-k_P(t - t_{eq})\} \quad \text{(Eq. 1)}$$

where k_P is the rate constant of the LfcinB-induced local rupture and t_{eq} is a fitting parameter that denotes the time required for the binding equilibrium of LfcinB from the aqueous solution to the GUV membrane. The experimental data of the time course of P_{intact} showed a good fit with the single exponential decay function defined by Equation 1. To determine the mean value for k_P, two independent experiments ($n = 2$) using 12–15 single GUVs to obtain the time course of P_{intact} were carried out, and these curves also showed a good fit by Equation 1. The mean ± S.D. of k_P for 40 μM LfcinB was $(8 \pm 3) \times 10^{-3}$ s^{-1} ($n = 2$). Fig. 5*E* (▲) indicated that the k_P increased with an increase in LfcinB concentration. Fig. 5*E* (red ■) also revealed that the fraction of leaked GUV among all examined GUVs (P_{leak} [$=1 - P_{intact}$]) after 10 min (*i.e.* P_{leak} (10 min)) increased with an increase in LfcinB concentration. At less than 5 μM LfcinB, no leakage of AF647 was observed, indicating that local rupture did not occur in *E. coli*-lipid-GUVs at low LfcinB concentrations.

Measurement of the membrane potential of GUVs using a fluorescent probe

As described in the previous section, LfcinB induced rapid, stochastic leakage of AF647 from single *E. coli*-lipid-GUVs;

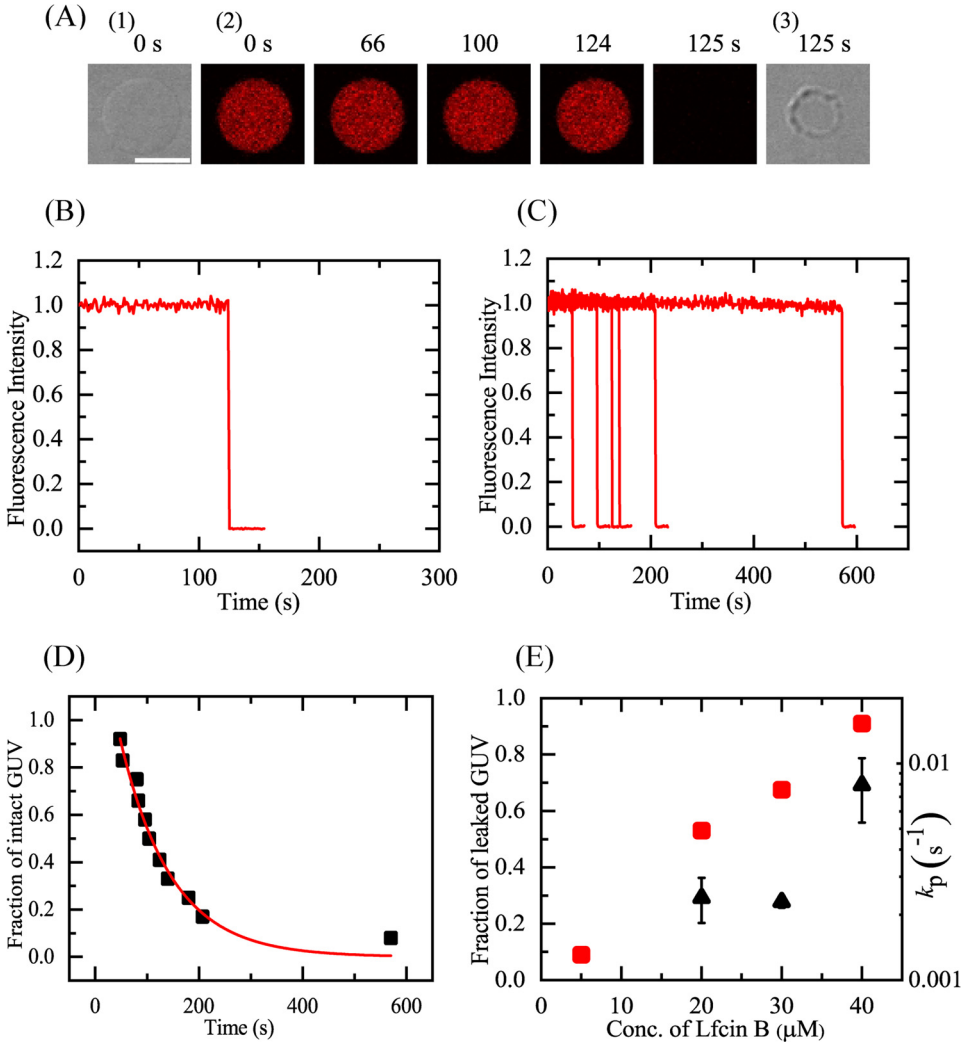

Figure 5. LfcinB-induced leakage of AF647 from single *E. coli*-lipid-GUVs. *A,* leakage of AF647 from single *E. coli*-lipid-GUVs induced by 40 μM LfcinB in buffer C at 25 °C. CLSM images (*2*) show that the AF647 concentration inside the GUV rapidly decreased after some lag time of the addition of LfcinB. The *numbers above* each image show the time in seconds after the LfcinB addition was started. Also shown are DIC images of the GUV at time 0 (*1*) and 125 s (*3*). The *bar* corresponds to 20 μm. *B,* time course of the change in the normalized FI of the GUV shown in *A*. We obtained the normalized FI of a GUV as the ratio of the FI at time *t* to that before the addition of LfcinB. *C,* other examples of the time course of the change in the normalized FI of several single GUVs under the same conditions as in *A*. Each curve corresponds to the time course of each GUV. *D,* time course of fraction of intact GUV, P_{intact}, among all examined GUVs. The *solid line* represents the best fit curve of Equation 1. *E,* LfcinB concentration dependence of the rate constant of local rupture, k_p (▲), and fraction of leaked GUV at 10 min (*red* ■). Mean ± S.D. of these values are shown.

however, higher concentrations of LfcinB were required to induce a significant rate of local rupture in GUVs compared with *E. coli* cells and spheroplasts. On the other hand, the results shown in Figs. 2 and 4 indicate that the membrane potential across the plasma membrane of *E. coli* cells and spheroplasts increases the rate of LfcinB-induced pore formation or local rupture of the plasma membrane. Based on these results, we inferred that membrane potential may increase the rate of LfcinB-induced local rupture in *E. coli*-lipid-GUVs. To test this hypothesis, we examined the effect of membrane potential on LfcinB-induced leakage from single *E. coli*-lipid-GUVs.

To apply a membrane potential across a GUV membrane, we included a small amount of gramicidin A in the GUV membrane and generated a difference in K^+ concentration between the lumen and the outside of the GUVs by diluting GUVs prepared in buffer K (containing 50 mM KCl) with buffer T (containing 50 mM tetraethylammonium chloride (TEAC)) at various ratios. It is well-known that gramicidin A is a small ion channel for monovalent cations (36, 37), and tetraethylammonium ions (TEA^+) cannot permeate through the gramicidin A channel nor block the channel (38). Therefore, only the ratio of the K^+ concentration in the outside of a GUV, $[K^+]_{out}$, to that in the GUV lumen, $[K^+]_{in}$, determines the membrane potential, $\Delta\varphi$, according to the Nernst equation (*i.e.* Equation 2 under "Experimental procedures"). For example, when $[K^+]_{in} = 50$ mM, $\Delta\varphi = -59$ mV for $[K^+]_{out} = 5.0$ mM, and $\Delta\varphi = -102$ mV for $[K^+]_{out} = 0.94$ mM at 25 °C.

To detect a change in the membrane potential produced by various K^+ gradients across GUV membranes, we examined the interaction of 1 nM of the membrane potential-sensitive dye 3,3′-dihexyloxacarbocyanine iodide ($DiOC_6(3)$) with *E. coli*-lipid-GUVs at various membrane potentials using CLSM. Fig. 6*A* shows representative CLSM images of one of the *E. coli*-

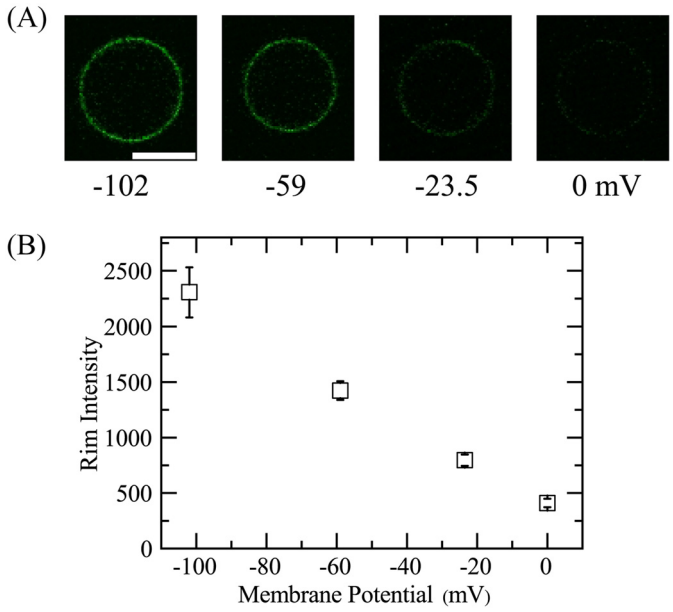

Figure 6. Effects of membrane potential on the rim intensity due to $DiOC_6(3)$ in single *E. coli*-lipid-GUVs. *A,* CLSM images of the GUV obtained using the fluorescence emitted by $DiOC_6(3)$. The *number below* each image shows the membrane potential on the GUV membrane (from 0.0 to −102 mV). The *bar* corresponds to 20 μm. *B,* dependence of rim intensity of single GUVs on membrane potential at 25 °C. The mean ± S.D. of the rim intensity are shown.

lipid-GUVs under various membrane potentials. The FI of the GUV membrane (*i.e.* the rim intensity of the GUV) due to $DiOC_6(3)$ increased with an increase in negative membrane potential (or the absolute value of membrane potential) (Fig. 6, *A* and *B*).

It is thought that $DiOC_6(3)$ can enter the cytoplasm of cells under negative potentials by translocating across the plasma membranes and hence the $DiOC_6(3)$ concentration in the cytoplasm increases (39–42). In the case of GUVs, with an increase in negative membrane potential, the $DiOC_6(3)$ concentration in the GUV lumen becomes larger than that in the outside of the GUV. The binding equilibrium of $DiOC_6(3)$ between the GUV lumen and inner monolayer of the GUV holds, and thus, the $DiOC_6(3)$ concentration in the inner leaflet of the GUV increases with an increase in negative membrane potential. It can be reasonably inferred that the rim intensity due to $DiOC_6(3)$ is proportional to the $DiOC_6(3)$ concentration in the GUV membrane at a low concentration, although at higher $DiOC_6(3)$ concentrations the rim intensity would decrease due to quenching of $DiOC_6(3)$ (39). Therefore, Fig. 6 indicates qualitatively that the $DiOC_6(3)$ concentration in the GUV membrane increased with an increase in membrane potential (calculated by the Nernst equation), *i.e.* with an increase in the K^+ concentration gradient. We can reasonably infer that the binding constant of $DiOC_6(3)$ from aqueous solution to lipid monolayers is large because $DiOC_6(3)$ has two hydrocarbon chains per molecule, and thus, most $DiOC_6(3)$ dyes exist in the membrane, not in aqueous solution of the GUV lumen. Therefore, the sensitivity of detection of membrane potential in the measurement of the rim intensity is greater than that in the measurement of FI of GUV lumen. The result shown in Fig. 6 also indicates that the GUVs prepared using our method showed negative membrane potentials and their absolute value increased with a decrease in K^+ concentration in the outside of a GUV, $[K^+]_{out}$. Hence, we can use these GUVs to investigate the effect of membrane potential on the LfcinB-induced local rupture of GUVs.

Effect of membrane potential on the interaction of LfcinB with single E. coli-lipid-GUVs

We examined the effect of membrane potential ($\Delta\varphi$) on the interaction of 5.0 μM LfcinB with single *E. coli*-lipid-GUVs (Fig. 7). In the absence of membrane potential, 5.0 μM LfcinB induced leakage of AF647 from single *E. coli*-lipid-GUVs with a low probability, *i.e.* the fraction of leaked GUV at 10 min was 0.09 (Fig. 5*E*). First, we investigated the effect of $\Delta\varphi = -102$ mV. After applying $\Delta\varphi = -102$ mV to the GUVs, the LfcinB solution was continuously provided to the vicinity of the GUV through a micropipette under confocal microscope. The FI of the GUV lumen due to AF647 remained essentially constant during the addition of LfcinB solution for the first 50 s, then the FI rapidly decreased (Fig. 7, *A* and *B*). At 51 s, the FI fell to effectively zero; a DIC image of the same GUV (Fig. 7*A*(3)) showed that the spherical GUV structure remained, albeit with an apparent decrease in diameter. The time at which the FI began to rapidly decrease corresponded to the time at which local rupture occurred in the GUV. When the same experiments were carried out using 15 single GUVs, we observed the stochastic occurrence of a similar rapid leakage of AF647 from each GUV (Fig. 7*C*). Fig. 7*D* shows that the P_{intact} of *E. coli*-lipid-GUVs decreased with time in the presence of 5.0 μM LfcinB, which was fit with the single exponential decay function defined by Equation 1. To determine the mean value for k_P, two independent experiments ($n = 2$) using 12–15 single GUVs to obtain the time course of P_{intact} were carried out and these data were also fit well with Equation 1. The mean value of k_P for 5.0 μM LfcinB at $\Delta\varphi = -102$ mV was $(4.9 \pm 0.2) \times 10^{-3}$ s^{-1} ($n = 2$). We also examined the effect of various membrane potentials. For example, Fig. S2 shows the results at $\Delta\varphi = -86$ mV. Fig. 7*E* indicated that the k_P increased with an increase in negative membrane potential (or the absolute value of membrane potential). Fig. 7*F* indicated that the fraction of leaked GUV at 10 min also increased with membrane potential. At $\Delta\varphi = -102$ mV, the fraction of leaked GUV at 10 min increased in an LfcinB concentration-dependent manner (Fig. 7*G*).

Discussion

The results in this study show that in the interaction of LfcinB with single *E. coli* cells and single *E. coli* spheroplasts, LfcinB induced rapid, complete leakage of calcein from the cytosol, indicating that LfcinB induced rapid permeabilization due to local damage or pore formation in the plasma membrane, through which calcein molecules rapidly leaked out. Therefore, we can conclude that the antimicrobial activity of LfcinB is mainly due to permeabilization in plasma membrane of *E. coli* cells induced by the direct interaction of LfcinB with the plasma membrane. In the interaction of LfcinB with single *E. coli*-lipid GUVs, LfcinB induced rapid, stochastic leakage of AF647 due to local rupture of the GUVs; however, higher LfcinB concentrations were required to induce a significant rate

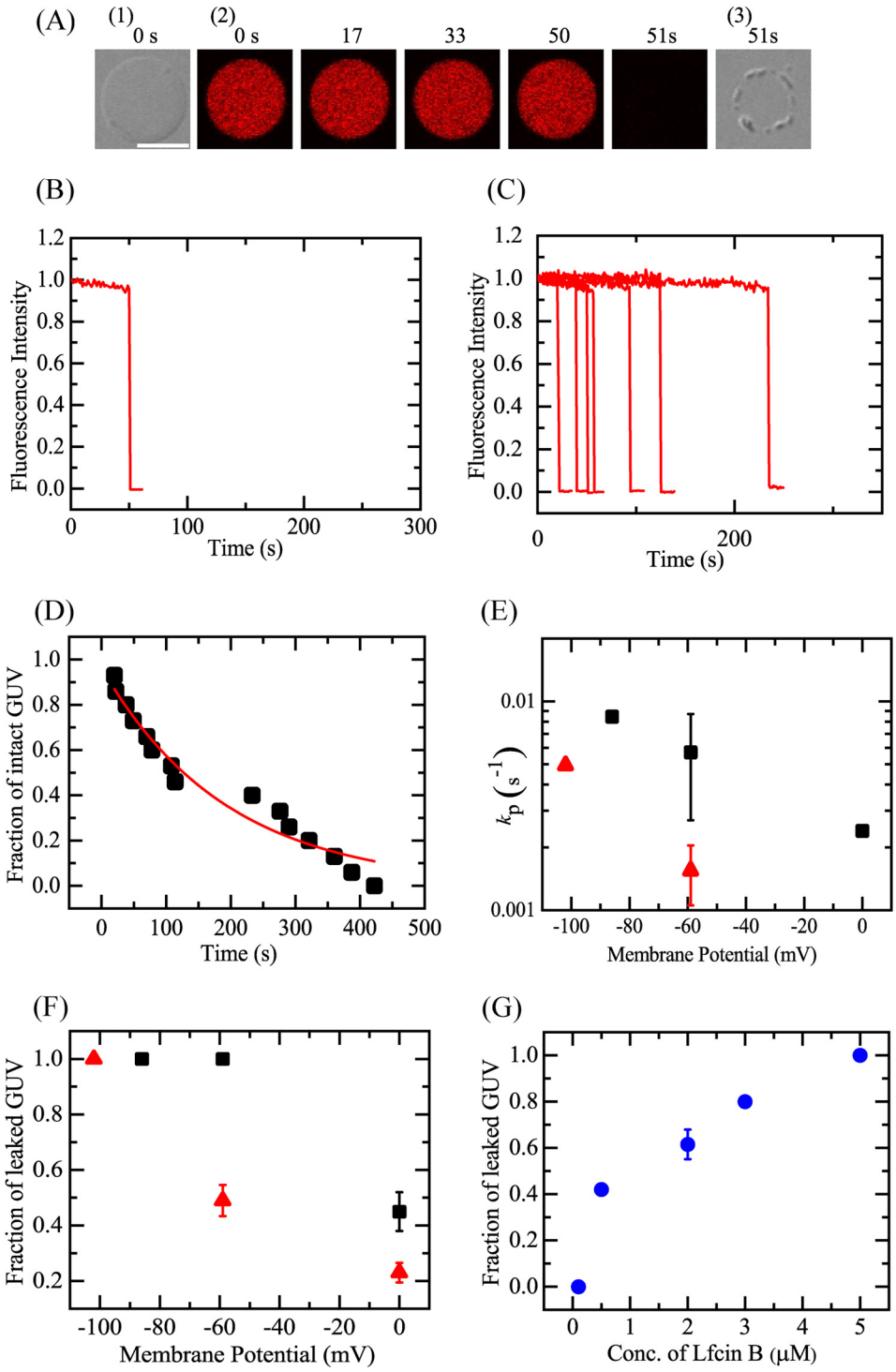

Figure 7. LfcinB-induced leakage of AF647 from single *E. coli*-lipid-GUVs under membrane potential, $\Delta\varphi$. *A,* leakage of AF647 from single *E. coli*-lipid-GUVs with $\Delta\varphi = -102$ mV induced by 5 μM LfcinB at 25 °C. CLSM images (*2*) show that the AF647 concentration inside the GUV rapidly decreased after some lag time of the addition of LfcinB. The *numbers above* each image show the time in seconds after the LfcinB addition was started. Also shown are DIC images of the GUV at time 0 (*1*) and 51 s (*3*). The *bar* corresponds to 20 μm. *B,* time course of the change in the normalized FI of the GUV shown in *A*. We obtained the normalized FI of a GUV as the ratio of the FI at time *t* to that before the addition of LfcinB. *C,* other examples of the time course of the change in the normalized FI of several single GUVs under the same conditions as in *A*. Each curve corresponds to the time course of each GUV. *D,* time course of fraction of intact GUV, P_{intact}, among all examined GUVs. The *solid line* represents the best fit curve of Equation 1. *E,* membrane potential dependence of the rate constant of pore formation, k_P. Mean ± S.D. values of k_P are shown (*red* ▲, 5 μM, and ■, 20 μM LfcinB). *F,* dependence of fraction of leaked GUV at 10 min on membrane potential (*red* ▲, 5 μM, and ■, 20 μM LfcinB). *G,* dependence of the fraction of leaked GUV at 10 min under $\Delta\varphi = -102$ mV on LfcinB concentration.

of permeabilization compared with that observed in *E. coli* cells and spheroplasts. This result indicates other factors are necessary to induce LfcinB-induced rapid local rupture in *E. coli*-lipid-GUVs. We considered membrane potential as one of these factors. We found that the rate constant of LfcinB-induced local rupture in GUVs increased greatly with an increase

in negative membrane potential, and at $\Delta\varphi = -102$ mV, the rate of local rupture at the same LfcinB concentrations became similar in the GUVs and *E. coli* cells. In the case of the interaction of LfcinB on single spheroplasts and *E. coli* cells, the CCCP-induced dissipation of membrane potential greatly decreased the rate of permeabilization in the plasma membrane. To the best of our knowledge, this is the first report that indicates the significant role of membrane potential in the permeabilization activity of AMPs in GUVs of lipid bilayers and spheroplasts, whereas some researchers have suggested the role of membrane potential in the interaction of AMPs with bacterial cells (43, 44).

Some previous results have suggested the effects of membrane potential on AMP activities. Yeaman and colleagues (43) found that the activity of platelet microbicidal protein-2 (PMP-2) to induce permeabilization against *Staphylococcus aureus* strain 6850 with $\Delta\varphi = -150$ mV was greater than that against another *S. aureus* strain (JB-1) with $\Delta\varphi = -100$ mV, indicating that $\Delta\varphi$ plays an important role in the antimicrobial activity of PMP-2 against *S. aureus*. Hancock and colleagues (44) found that in the interaction of AMPs with planar bilayers, high transmembrane voltage (usually −180 mV) was indispensable to induce conductance, and the increase in KCl concentration in the outside of *E. coli* cells (*i.e.* decrease in $\Delta\varphi$) did not alter the antimicrobial activity of several α-helical cationic peptides and a β-structured peptide (Gram 474) (judging from MIC values) but decreased the antimicrobial activity of gramicidin S, Gram 4112, and indolicidin (44), suggesting that $\Delta\varphi$ plays an important role in the antimicrobial activity of some AMPs.

Recently, it is well-recognized that membrane potential greatly affects the localization of many proteins in bacterial cells (34). Therefore, the results of the effects of the change in membrane potential on activities of AMPs in bacterial cells can be interpreted by various ways. For example, a change in localization of a specific protein in the cells may affect the activity of AMPs. However, the results in this study show that membrane potential greatly affects the activity of LfcinB in *E. coli* spheroplasts, indicating that the effect of membrane potential on the interaction of LfcinB with the plasma membrane (neither periplasm nor outer membrane) of bacterial cells plays an important role in the LfcinB-induced leakage. Moreover, the results in this study show that the negative membrane potential greatly increases the activity of LfcinB in *E. coli*-lipid-GUVs, indicating that the effect of membrane potential on the interaction of LfcinB with lipid bilayer regions of the plasma membrane of bacterial cells plays a vital role in the LfcinB-induced leakage. Therefore, to the best of our knowledge, this is the first report to indicate that membrane potential plays a vital role in the interaction of AMPs with lipid bilayer regions of the plasma membrane of bacterial cells to induce their bactericidal activity.

In this study, we observed the interaction of LfcinB with single cells, and hence, we detected variations of the LfcinB-induced permeabilization of the plasma membrane of each cell. For low concentrations of LfcinB (*e.g.* 3.0 μM), the rates of LfcinB-induced leakage from septating cells were larger than those from most nonseptating cells and the rate of LfcinB-induced leakage of calcein from single nonseptating *E. coli* cells exhibited a wide distribution (Fig. 1*E* and Fig. S1). Generally, the rate of leakage depends on degree of the damage, such as pore formation induced by peptides/proteins in lipid membranes and plasma membrane, such as the size and the number of pores or local rupture (45, 46). Therefore, the rate of permeabilization in plasma membrane depends on AMP concentration in the membrane and the degree of interaction of AMPs with the membrane. We can reasonably consider that each *E. coli* cell exists in a different step of the bacterial cell cycle (*e.g.* replication, Z-ring formation, end of replication, septation, division) (47, 48). The degree of damage in the plasma membrane induced by LfcinB may greatly depend on the step of cell cycle of *E. coli* cells. In the cell cycle, only the septating cells are clearly recognized from their optical microscopic images. The result that the rates of LfcinB-induced leakage from septating cells were larger than those from most nonseptating cells is evident, but currently its mechanism is not clear. Further investigation is required. In contrast, for the higher concentration of LfcinB (5.0 μM), the leakage started stochastically (*i.e.* the onset times of the leakage were random) but the rate of LfcinB-induced leakage of calcein was similar in all examined cells. This result suggests that the degree of the damage induced by LfcinB does not depend on the step of the cell cycle at a higher concentration of LfcinB.

At present, the mechanism of the effect of membrane potential on LfcinB-induced local rupture or pore formation in lipid bilayers of GUVs is not clear. We can expect that the negative membrane potential induces a large electric field inside the lipid bilayer, which could alter the interaction modes of LfcinB with the membrane, such as degree of insertion of peptides into the membrane interface, which may change the physical property of the membranes and their stretching. Further studies on the effect of membrane potential on the mechanisms of LfcinB-induced pore formation are indispensable.

In this study, we demonstrated that the electrochemical potential of proton or membrane potential plays a vital role in the activity of LfcinB (*i.e.* LfcinB-induced permeabilization) in bacterial cells and lipid vesicles by affecting the interaction of LfcinB with the membranes. So far almost all studies on the interactions of AMPs with lipid bilayers and the structures of AMPs in lipid bilayers have been performed in the absence of membrane potential. Therefore, it is indispensable to reconsider and reinterpret all the results obtained in these studies. Furthermore, we have to reveal the mechanisms of activities of AMPs by including the effects of membrane potential. Currently it is recognized that there are several modes of actions of AMPs (54). Thus, it is necessary to examine the effects of membrane potential on each mode of action of AMPs. To design new peptides that have an antimicrobial activity, it is indispensable to consider the effect of membrane potential on the interaction of the peptides with lipid bilayers.

Conclusion

The results of the effect of LfcinB on single *E. coli* cells and single spheroplasts indicate that the direct interaction of LfcinB with plasma membranes induced rapid permeabilization. We can reasonably consider that this permeabilization induced growth cessation of the cells, based on the results of changes in the cell length during LfcinB interaction with single cells. At

present it is not clear that this rapid permeabilization occurs due to large pore formation or local rupture in the plasma membrane. The presence of CCCP (hence the decrease in the membrane potential) suppressed this leakage. On the other hand, LfcinB induced local rupture in single *E. coli*-lipid-GUVs, through which AF647 leaked rapidly from the GUV lumen. The rate of this LfcinB-induced local rupture in single GUVs increased with an increase in negative membrane potential of the GUVs. These results indicate that the membrane potential plays an important role in LfcinB-induced local rupture of lipid bilayers and in the interaction of LfcinB with lipid bilayer regions of the plasma membrane of bacterial cells to induce rapid permeabilization, resulting in their bactericidal activity. The results in this study are indispensable in revealing the mechanism of action of LfcinB and also other AMPs against bacterial cells.

Experimental procedures

Materials

E. coli polar lipid extract was purchased from Avanti Polar Lipids, Inc. (Alabaster, AL). Bovine serum albumin (BSA) was purchased from Fuji Film Wako Pure Chemical Co. (Osaka, Japan). Alexa Fluor 647 hydrazide (AF647), calcein-acetoxymethyl (calcein-AM), and $DiOC_6(3)$ were purchased from Thermo Fisher Scientific (Waltham, MA). Cephalexin, poly-L-lysine, deoxyribonuclease I (DNase I), lysozyme, and CCCP were purchased from Sigma. TEAC was purchased from Tokyo Chemical Industry Co., Ltd., (Tokyo, Japan). EZ Rich Defined Medium (EZ rich medium) was purchased from TEKnova (Hollister, CA).

Peptide synthesis and identification

LfcinB with an amide-blocked C terminus was synthesized by the FastMoc method using a 433A peptide synthesizer (PE Applied Biosystems, Foster City, CA) (18). The methods of cleavage, peptide purification, and measurement of mass have been described previously (18). LfcinB concentration in buffer was determined by absorbance using the molar extinction coefficient of Trp at 278 nm (*i.e.* 5,500 M^{-1} cm^{-1}).

CLSM investigation of the interaction of LfcinB with single E. coli cells containing calcein

An *E. coli* (JM-109) suspension was subcultured on nutrient agar plates at 37 °C overnight to obtain single colonies, and a single bacterial colony was then grown in Nutrient Broth medium for 6 to 7 h (exponential phase cells) (18). The bacterial suspension was diluted to obtain a final bacterial concentration of 1×10^6 CFU/ml, which was pelleted by centrifugation (620 × *g*, 10 min); the pellet was washed and resuspended in EZ rich medium (containing 50 mM NaCl and 1.3 mM K_2HPO_4 as main ion sources (28)). Calcein loading of *E. coli* was performed according to the method of Dubey and Ben-Yehuda (29). In brief, a 50-μl aliquot of calcein-AM (1.0 μg/μl in DMSO solution) was added into 1.0 ml of the bacteria suspension, which was shaken using a rotary shaker for 2 h at room temperature under darkness. Then, the suspension was centrifuged at 620 × *g* for 10 min, and the pellet was resuspended in fresh EZ rich medium. This procedure was repeated twice. The *E. coli* suspension was transferred into a handmade chamber formed on a glass slide by putting a U-shaped silicone-rubber spacer between the glass slide and a coverslip (18), and *E. coli* cells had settled onto the coverslip surface after 15 min and were adsorbed thereafter. To fix live *E. coli* cells to the glass surface of coverslips, we generated poly-L-lysine coatings on coverslips using the standard method.

Interactions of LfcinB with single *E. coli* cells containing calcein were observed under a confocal laser scanning microscope (FV-1000, Olympus, Tokyo, Japan) at 25 ± 1 °C with a stage thermocontrol system (Thermoplate, Tokai Hit, Shizuoka, Japan), in reference to a previously reported method (30). For CLSM measurements, fluorescence images of calcein (473 nm laser) and DIC images were obtained using a ×60 objective (UPLSAPO060X0, Olympus) (NA = 1.35) (25, 30). During interaction of the peptide with single *E. coli* cells, various concentrations of LfcinB in the medium were added continuously to the vicinity of the single *E. coli* cells through a 20-μm diameter glass micropipette positioned by a micromanipulator (18, 31). The distance between the single cells and the tip of the micropipette was 50 μm, and the applied pressure, ΔP ($= P_{in} - P_{out}$, where P_{in} and P_{out} are the pressure of the inside and outside of a micropipette, respectively) was 30 pascals. ΔP was measured using a differential pressure transducer (DP15, Validyne, Northridge, CA), pressure amplifier (PA501, Validyne), and a digital multimeter. Glass micropipettes were prepared by pulling 1.0-mm glass capillaries composed of borosilicate glass (G-1, Narishige, Tokyo, Japan) using a puller (PC-10, Narishige). Details of these methods have been described previously (31, 49).

For the experiments of the interaction of LfcinB with single *E. coli* cells in the presence of CCCP in the EZ medium, we mixed CCCP solution in EZ media containing DMSO with the suspension of *E. coli* cells containing calcein (final concentrations were 100 μM CCCP, 0.5% DMSO, and 1×10^6 CFU/ml *E. coli* cells), and then transferred this mixture into a handmade chamber. After more than 10 min incubation, we investigated the interaction of LfcinB with single *E. coli* cells.

CLSM investigation of the interaction of LfcinB with single spheroplasts containing calcein

Spheroplasts of *E. coli* cells were prepared using a similar method to Martinac *et al.* (21). Details of the method are described in the supporting data. In brief, first, single-cell filaments were prepared by growing *E. coli* cells in the presence of cephalexin, which prevents cell division (50–52). For hydrolysis of the peptidoglycan layer, the single-cell filaments were reacted with lysozyme, DNase I, and EDTA. $MgCl_2$ was added to stop the reaction. Finally, $MgCl_2$ was replaced with KCl and NaCl because Mg^{2+} affected the interaction of LfcinB with spheroplasts. The final buffer of the purified spheroplasts was 10 mM Tris-HCl (pH 7.8) containing 1.5 mM KCl, 48.5 mM NaCl, and 0.73 M sucrose. We used these spheroplasts within 3 h after the purification, without storing in the freezer.

For calcein loading to spheroplasts, we used a similar method of loading calcein in *E. coli* cells (29). A 50-μl aliquot of calcein-AM (1.0 μg/μl in DMSO solution) was added to 1.0 ml of

a spheroplast suspension (final DMSO concentration was 1%), which was incubated for 30 min at room temperature under darkness. Then, the suspension was transferred into a microchamber and used in the interaction of LfcinB under a confocal laser scanning microscope. The interaction of LfcinB with single spheroplasts containing calcein was investigated at 25 ± 1 °C using a method similar to that used for single *E. coli* cells, as described in the above section.

For the experiments of the interaction of LfcinB with single spheroplasts in the presence of CCCP, we mixed a CCCP solution in the same buffer containing DMSO with the suspension of spheroplasts containing calcein (final concentrations are 100 μM CCCP and 0.5% DMSO), and then transferred this mixture into a handmade chamber. After more than 10 min incubation, we investigated the interaction of LfcinB with single spheroplasts.

GUV preparation

GUVs of *E. coli* polar lipid extract (*E. coli*-lipid-GUVs) were prepared by incubating buffer C (10 mM PIPES, pH 7.0, 1 mM EGTA, 50 mM NaCl) containing 0.10 M sucrose and 6.0 μM AF647 with dry lipid films by the natural swelling method at 37 °C for 2–3 h (18). The membrane filtering method was used to remove untrapped fluorescent probes (53).

Purified GUV suspension (300 μl: 0.1 M sucrose in buffer C as the internal solution; 0.1 M glucose in buffer C as the external solution) was transferred into a handmade microchamber (18). To prevent strong interaction between the glass surface and GUVs, the inside of the microchamber was coated with 0.10% (w/v) BSA in buffer C containing 0.10 M glucose (18).

CLSM investigation of the interaction of LfcinB with single E. coli-lipid-GUVs

GUVs were observed using a confocal laser scanning microscope (FV-1000, Olympus) at 25 ± 1 °C using a stage thermocontrol system (Thermoplate, Tokai Hit). For CLSM measurements, fluorescence images of AF647 (excited by a laser at λ = 635 nm) and DIC images were obtained using the ×60 objective (19, 30, 39). To investigate the effect of LfcinB on single GUVs, various concentrations of LfcinB in buffer C containing 0.10 M glucose were added continuously to the vicinity of the GUV through a 20-μm diameter glass micropipette positioned using a micromanipulator. The distance between the single cells and the tip of the micropipette was 50 μm, and the applied pressure, Δ*P*, was 30 pascals (31). Consequently, the LfcinB concentration near the GUV approached steady state and was almost the same as the concentration inside the micropipette (31).

Application of membrane potential to single GUVs

To induce a membrane potential in GUVs, we created a K^+ concentration gradient across the GUV membrane. To induce permeability of K^+ in the GUV membrane, gramicidin A molecules were incorporated in the GUV membrane. For this purpose, we prepared GUVs of *E. coli*-lipid/gramicidin A (molar ratio: 100/0.01) from a dry lipid film in buffer K (10 mM PIPES, pH 7.0, 50 mM KCl, and 1 mM EGTA) containing 0.10 M sucrose and 6.0 μM AF647 by the natural swelling method, and purified them by the membrane filtering method. Then, we diluted the purified GUV suspension with buffer T (10 mM PIPES, pH 7.0, 50 mM TEAC, and 1 mM EGTA) containing 0.1 M glucose at various ratios. The total concentration of KCl and TEAC in the buffer outside the GUVs was 50 mM, which had the same osmotic pressure as the buffer inside the GUVs. The membrane potential difference across a GUV membrane, Δφ, or the membrane potential inside a GUV, φ_{in}, was measured using the following Nernst equation,

$$\Delta\varphi = \frac{RT}{F}\ln\frac{[K^+]_{out}}{[K^+]_{in}} = 25.7\ln\frac{[K^+]_{out}}{[K^+]_{in}}(\text{mV}) \qquad \text{(Eq. 2)}$$

where *F* is the Faraday constant, *R* is the gas constant, *T* is the absolute temperature, $[K^+]_{out}$ and $[K^+]_{in}$ are the K^+ concentrations outside and inside the GUV, respectively. The numerical value (25.7) in the last equation in Equation 2 is for 25 °C. For example, when we diluted the GUV suspension with buffer T at a GUV suspension to buffer T ratio of 1:9, Δφ = −59 mV at 25 °C. To investigate the interaction of LfcinB with single GUVs with various membrane potentials, we used the same method described in the above section. We used the same buffer mixture to prepare LfcinB solution as for the outside of the GUVs. We waited 10 min after application of the K^+ gradient to attain an equilibrium, and the GUVs were observed using CLSM.

We also measured the membrane potential using a fluorescent probe, $DiOC_6(3)$, which is sensitive to the membrane potential (39–42). First, we mixed the membrane potential probe $DiOC_6(3)$ in methanol solution with the buffer, which was the same as for the outside of the GUVs, and then mixed this $DiOC_6(3)$ solution in the buffer with a suspension of GUVs with a membrane potential that had been produced due to a K^+ concentration gradient across the GUV membrane. The final concentrations were 1 nM $DiOC_6(3)$ and 0.006% methanol. Then, the GUV suspension was transferred into a handmade microchamber. To prevent strong interaction between the glass surface and the GUVs, the inside of the microchamber was coated with 0.10% (w/v) BSA in the same buffer as used for the experiments. We waited 10 min after the application of the K^+ gradient to attain an equilibrium, and the GUVs were observed using a confocal laser scanning microscope (FV-1000) at 25 ± 1 °C using the stage thermocontrol system (Thermoplate). Fluorescence images of $DiOC_6(3)$ (excited by a laser at λ = 473 nm) and DIC images were obtained using the ×60 objective. The fluorescence intensities of the images obtained by CLSM were measured using the software supplied with the CLSM (Fluoview, version 4.1, Olympus). The fluorescence intensity of the rim of a GUV due to the binding of $DiOC_6(3)$ dye was measured as the peak intensity in a line crossing the GUV (19).

We investigated the interaction of LfcinB with single *E. coli*-lipid-GUVs with various membrane potentials using the same method described in the above section (CLSM investigation of the interaction of LfcinB with single *E. coli*-lipid-GUVs). Various concentrations of LfcinB in the same buffer as for the outside of the GUVs (*i.e.* mixture of buffer T and buffer K with various ratios) containing 0.10 M glucose were added continuously to the vicinity of the GUV through a 20-μm diameter glass micropipette positioned using a micromanipulator.

Author contributions—F. H. and M. Y. conceptualization; F. H. and M. Y. data curation; F. H. and M. Y. formal analysis; F. H., M. M. R. M., M. Z. I., M. M., and M. Y. investigation; F. H. and M. Y. visualization; F. H., M. M. R. M., M. Z. I., M. M., and M. Y. methodology; F. H. and M. Y. writing-original draft; F. H., M. M. R. M., M. Z. I., and M. Y. writing-review and editing; M. Y. resources; M. Y. software; M. Y. supervision; M. Y. funding acquisition; M. Y. validation; M. Y. project administration.

References

1. Bellamy, W., Takase, M., Yamauchi, K., Wakabayashi, H., Kawase, K., and Tomita, M. (1992) Identification of the bacterial domain of lactoferrin. *Biochim. Biophys. Acta* **1121,** 130–136 CrossRef Medline
2. Kuwata, H., Yip, T. T., Tomita, M., and Hutchens, T. W. (1998) Direct evidence of the generation in human stomach of an antimicrobial peptide domain (lactoferricin) from ingested lactoferrin. *Biochim. Biophys. Acta* **1429,** 129–141 CrossRef Medline
3. Yamauchi, K., Tomita, M., Giehl, T. J., Ellison, R. T., 3rd (1993) Antibacterial activity of lactoferrin and a pepsin-derived lactoferrin peptide fragment. *Infect. Immun.* **61,** 719–728 Medline
4. Tomita, M., Takase, M., Bellamy, W., and Shimamura, S. (1994) A review: the active peptide of lactoferrin. *Acta Paediatr. J.* **36,** 585–591 CrossRef
5. Hwang, P. M., Zhou, N., Shan, X., Arrowsmith, C. H., and Vogel, H. J. (1998) Three-dimensional solution structure of lactoferricin B, an antimicrobial peptide derived from bovine lactoferrin. *Biochemistry* **37,** 4288–4298 CrossRef Medline
6. Hwang, P. M., and Vogel, H. J. (1998) Structure-function relationships of antimicrobial peptides. *Biochem. Cell Biol.* **76,** 235–246 CrossRef Medline
7. Zasloff, M. (2002) Antimicrobial peptides of multicellular organisms. *Nature* **415,** 389–395 CrossRef Medline
8. Yeaman, M. R., and Yount, N. Y. (2003) Mechanisms of antimicrobial peptide action and resistance. *Pharmacol. Rev.* **55,** 27–55 CrossRef
9. Hancock, R. E. W., and Hans-Georg, S. (2006) Antimicrobial and host-defense peptides as new anti-infective therapeutic strategies. *Nat. Biotech.* **24,** 1551–1557 CrossRef
10. Melo, M. N., Ferre, R., and Castanho, A. R. B. (2009) Antimicrobial peptides: linking partition, activity and high membrane-bound concentrations, *Nat. Rev. Microbiol.* **8,** 1–5
11. Kang, J. H., Lee, M. K., Kim, K. L., and Hahm, K.-S. (1996) Structure-biological activity relationships of 11-residue highly basic peptide segment of bovine lactoferrin. *Int. J. Pept. Protein Res.* **48,** 357–363 Medline
12. Schibli, D. J., Epand, R. F., Vogel, H. J., and Epand, R. M. (2002) Tryptophan-rich antimicrobial peptides: comparative properties and membrane interactions. *Biochem. Cell Biol.* **80,** 667–677 CrossRef Medline
13. Strøm, M. B., Haug, B. E., Rekdal, O., Skar, M. L., Stensen, W., and Svendsen, J. S. (2002) Important structural features of 15-residue lactoferricin derivatives and methods for improvement of antimicrobial activity. *Biochem. Cell Biol.* **80,** 65–74 CrossRef Medline
14. Nguyen, L. T., Schibli, D., and Vogel, H. J. (2005) Structural studies and model membrane interactions of two peptides derived from lactoferricin. *J. Peptide Sci.* **11,** 379–389 CrossRef
15. Gifford, J. L., Hunter, H. N., and Vogel, H. J. (2005) Lactoferricin: a lactoferrin-derived peptide with antimicrobial, antiviral, antitumor, and immunological properties. *Cell. Mol. Life. Sci.* **62,** 2588–2598 CrossRef Medline
16. Wakabayashi, H., Matsumoto, H., Hashimoto, K., Teraguchi, S., Takase, M., and Hayasawa, H. (1999) *N*-Acylated and D enantiomer derivatives of a nonamer core peptide of lactoferricin B showing improved antimicrobial activity. *Antimicrob. Agents Chemother.* **43,** 1267–1269 CrossRef
17. Wakabayashi, H., Takase, M., and Tomita, M. (2003) Lactoferricin derived from milk protein lactoferrin. *Curr. Pharm. Des.* **9,** 1277–1287 CrossRef Medline
18. Moniruzzaman, M., Alam, J. M., Dohra, H., and Yamazaki, M. (2015) Antimicrobial peptide lactoferricin B-induced rapid leakage of internal contents from single giant unilamellar vesicles. *Biochemistry* **54,** 5802–5814 CrossRef Medline
19. Islam, M. Z., Alam, J. M., Tamba, Y., Karal, M. A. S., and Yamazaki, M. (2014) The single GUV method for revealing the functions of antimicrobial, pore-forming toxin, and cell-penetrating peptides or proteins. *Phys. Chem. Chem. Phys.* **16,** 15752–15767 CrossRef Medline
20. Ruthe, H.-J., and Adler, J. (1985) Fusion of bacterial spheroplasts by electric fields. *Biochem. Biophys. Acta* **819,** 105–113 CrossRef Medline
21. Martinac, B., Buechner, M., Delcour, A. H., Adler, J., and Kung, C. (1987) Pressure-sensitive ion channel in *Escherichia coli*. *Proc. Natl. Acad. Sci. U.S.A.* **84,** 2297–2301 CrossRef
22. Wei, L., LaBouyer, M. A., Darling, L. E. O., and Elmore, D. E. (2016) Bacterial spheroplasts as a model for visualizing membrane translocation of antimicrobial peptides. *Antimicrob. Agents Chemother.* **60,** 6350–6352 CrossRef
23. Sun, Y., Sun, T.-L., and Huang, H. W. (2016) Mode of action of antimicrobial peptides on *E. coli* spheroplasts. *Biophys. J.* **111,** 132–139 CrossRef Medline
24. Tamba, Y., and Yamazaki, M. (2005) Single giant unilamellar vesicle method reveals effect of antimicrobial peptide Magainin 2 on membrane permeability. *Biochemistry* **44,** 15823–15833 CrossRef Medline
25. Islam, M. Z., Ariyama, H., Alam, J. M., and Yamazaki, M. (2014) Entry of cell-penetrating peptide transportan 10 into a single vesicle by translocating across lipid membrane and its induced pores. *Biochemistry* **53,** 386–396 CrossRef Medline
26. Hasan, M., Karal, M. A. S., Levadnyy, V., and Yamazaki, M. (2018) Mechanism of initial stage of pore formation induced by antimicrobial peptide magainin 2. *Langmuir* **34,** 3349–3362 CrossRef Medline
27. Felle, H., Porter, J. S., Slayman, C. L., and Kaback, H. R. (1980) Quantitative measurements of membrane potential in *Escherichia coli*. *Biochemistry* **19,** 3585–3590 CrossRef Medline
28. Neidhardt, F. C., Bloch, P. L., and Smith, D. F. (1974) Culture medium for enterobacteria. *J. Bacteriol.* **119,** 736–747 Medline
29. Dubey, G. P., and Ben-Yehuda, S. (2011) Intercellular nanotubes mediate bacterial communication. *Cell* **144,** 590–600 CrossRef Medline
30. Moniruzzaman, M., Islam, M. Z., Sharmin, S., Dohra, H., and Yamazaki, M. (2017) Entry of a six-residue antimicrobial peptide derived from lactoferricin B into single vesicles and *Escherichia coli* cells without damaging their membranes. *Biochemistry* **56,** 4419–4431 CrossRef Medline
31. Karal, M. A. S., Alam, J. M., Takahashi, T., Levadny, V., and Yamazaki, M. (2015) Stretch-activated pore of antimicrobial peptide magainin 2. *Langmuir* **31,** 3391–3401 CrossRef Medline
32. Tamba, Y., and Yamazaki, M. (2009) Magainin 2-induced pore formation in membrane depends on its concentration in membrane interface. *J. Phys. Chem. B* **113,** 4846–4852 CrossRef Medline
33. Sochacki, K. A., Barns, K. J., Bucki, R., and Weisshaar, J. C. (2011) Real-time attack on single *Escherichia coli* cells by the human antimicrobial peptide LL-37. *Proc. Natl. Acad. Sci. U.S.A.* **108,** E77–E81 CrossRef Medline
34. Strahl, H., and Hamoen, L. W. (2010) Membrane potential is important for bacterial cell division. *Proc. Natl. Acad. Sci. U.S.A.* **107,** 12281–12286 CrossRef Medline
35. Daniels, C. J., Bole, D. G., Quay, S. C., and Oxender, D. L. (1981) Role for membrane potential in the secretion of protein into the periplasm of *Escherichia coli*. *Proc. Natl. Acad. Sci. U.S.A.* **78,** 5396–5400 CrossRef
36. Finkelstein, A., and Andersen, O. S. (1981) The gramicidin A channel: a review of its permeability characteristics with special reference to the single-file aspect of transport. *J. Membr. Biol.* **59,** 155–171 CrossRef
37. Hille, B. (1992) Ionic channels of excitable membranes. 2nd Ed., Sinauer Association Inc., Sunderland, MA
38. Andersen, O. S. (1983) Ion movement through gramicidin A channels: interfacial polarization effects on single-channel current measurements. *Biophys. J.* **41,** 135–146 CrossRef Medline
39. Waggoner, A. S. (1979) Dye indicators of membrane potential. *Annu. Rev. Biophys. Bioeng.* **8,** 47–68 CrossRef
40. Shapiro, H. M. (1994) Cell membrane potential analysis. *Methods Cell Biol.* **41,** 121–133 CrossRef Medline
41. Fulda, S., Scaffidi, C., Susin, S. A., Krammer, P. H., Kroemer, G., Peter, M. E., and Debatin, K.-M. (1998) Activation of mitochondria and release

of mitochondrial apoptogenic factors by betulinic acid. *J. Biol. Chem.* **273,** 33942–33948 CrossRef Medline
42. Ishihara, Y., and Shimamoto, N. (2006) Involvement of endonuclease G in nucleosomal DNA fragmentation under sustained endogenous oxidative stress. *J. Biol. Chem.* **281,** 6726–6733 CrossRef Medline
43. Yeaman, M. R., Bayer, A. S., Koo, S.-P., Foss, W., and Sullam, P. M. (1998) Platelet microbicidal proteins and neutrophil defensing disrupt the *Staphlococcus aureus* cytoplasmic membrane by distinct mechanism of action. *J. Clin. Invest.* **101,** 178–187 CrossRef Medline
44. Wu, M., Maier, E., Benz, R., and Hancock, R. E. (1999) Mechanism of interaction of different classes of cationic antimicrobial peptides with planar bilayers and with the cytoplasmic membrane of *Escherichia coli*. *Biochemistry* **38,** 7235–7242 CrossRef Medline
45. Alam, J. M., Kobayashi, T., and Yamazaki, M. (2012) The single giant unilamellar vesicle method reveals lysenin-induced pore formation in lipid membranes containing sphingomyelin. *Biochemistry* **51,** 5160–5172 CrossRef Medline
46. Tamba, Y., Ariyama, H., Levadny, V., and Yamazaki, M. (2010) Kinetic pathway of antimicrobial peptide magainin 2-induced pore formation in lipid membranes. *J. Phys. Chem. B* **114,** 12018–12026 CrossRef Medline
47. Kiviet, D. J., Nghe, P., Walker, N., Boulineau, S., Sunderlikova, V., and Tans, S. J. (2014) Stochasticity of metabolism and growth at the single-cell level. *Nature* **514,** 376–379 CrossRef Medline
48. Osella, M., Tans, S. J., and Lagomarsino, M. C. (2017) Step by step, cell by cell: quantification of the bacterial cell cycle. *Trends Microbiol.* **25,** 250–256 CrossRef
49. Yamazaki, M. (2008) The single GUV method to reveal elementary processes of leakage of internal contents from liposomes induced by antimicrobial substances. *Adv. Planar Lipid Bilayers Liposomes* **7,** 121–142 CrossRef
50. Rolinson, G. N. (1980) Effect of β-lactam antibiotics on bacterial cell growth rate. *J. Gen. Microbiol.* **120,** 317–323 Medline
51. Maki, N., Gestwicki, J. E., Lake, E. M., Kiessling, L. L., and Adler, J. (2000) Motility and chemotaxis of filamentous cells of *Escherichia coli*. *J. Bacteriol.* **182,** 4337–4342 CrossRef Medline
52. Renner, L. D., and Weibel, D. B. (2011) Cardiolipin microdomains localize to negatively curved regions of *Escherichia coli*. *Proc. Natl. Acad. Sci. U.S.A.* **108,** 6264–6269 CrossRef
53. Tamba, Y., Terashima, H., and Yamazaki, M. (2011) A membrane filtering method for the purification of giant unilamellar vesicles. *Chem. Phys. Lipids* **164,** 351–358 CrossRef Medline
54. Hasan, M., and Yamazaki, M. (2019) Elementary processes and mechanisms of interactions of antimicrobial peptides with membranes: single giant unilamellar vesicle studies. *Antimicrobiol Peptides: Basic for Clinical Application* (Matsuzaki, K., ed) pp. 17–32, Springer Nature, Singapore Pre. Ltd.